

Article

Stereoselective Synthesis of a Novel Series of Dispiro-oxindolopyrrolizidines Embodying Thiazolo[3,2-*a*] benzimidazole Motif: A Molecular Electron Density Theory Study of the Mechanism of the [3 + 2] Cycloaddition Reaction

 Assem Barakat ^{1,*} , Saeed Alshahrani ¹ , Abdullah Mohammed Al-Majid ¹ , Abdullah Saleh Alamarly ¹ , M. Ali ¹  and Mar Ríos-Gutiérrez ^{2,*} 
¹ Department of Chemistry, College of Science, King Saud University,

P.O. Box 2455, Riyadh 11451, Saudi Arabia; chemistry99y@gmail.com (S.A.);

amajid@ksu.edu.sa (A.M.A.-M.); alamarly1401@yahoo.com (A.S.A.); maly.c@ksu.edu.sa (M.A.)

² Department of Organic Chemistry, University of Valencia, Dr. Moliner 50, 46100 Burjassot, Valencia, Spain

* Correspondence: ambarakat@ksu.edu.sa (A.B.); m.mar.rios@uv.es (M.R.-G.)

Abstract: A one-pot multi-component reaction was employed for the stereoselective synthesis of a novel set of dispiro-oxindolopyrrolizidines analogs incorporating a thiazolo[3,2-*a*] benzimidazole scaffold based on the [3 + 2] cycloaddition (32CA) reaction approach. The desired novel dispiro-oxindolopyrrolizidines **9a–d** were achieved using the 32CA reaction of new ethylene derivatives based on thiazolo[3,2-*a*] benzimidazole moiety **seven** with thiazolidine derivatives **eight** and different substituted isatin compounds **5a–d** (R = H, Cl, NO₂, and Br). The final dispiro-oxindolopyrrolizidines cycloadducts were separated, purified, and fully characterized by means of a set of spectroscopic tools including IR, HNMR, CNMR, and MS. The Molecular Electron Density Theory (MEDT) was applied to explain the mechanism and stereoselectivity in the of the key 32CA reaction step. The reactive *pseudo(mono)radical* electronic structure of the in situ generated azomethine ylides and the high polar character of the corresponding 32CA reactions account for the low computed activation Gibbs free energies and total endo stereoselectivity of this kinetically controlled exergonic reaction. The computed relative Gibbs free activation energies of competitive reaction paths and regioisomers ratio distribution of 80:20 justify the major formation of **9a** via the most favorable *ortho/endo* reaction path.

Keywords: imidazo [2,1-*b*]thiazole; dispiro-oxindolopyrrolizidines; [3 + 2] cycloaddition reaction; MEDT study



Citation: Barakat, A.; Alshahrani, S.; Al-Majid, A.M.; Alamarly, A.S.; Ali, M.; Ríos-Gutiérrez, M. Stereoselective Synthesis of a Novel Series of Dispiro-oxindolopyrrolizidines Embodying Thiazolo[3,2-*a*] benzimidazole Motif: A Molecular Electron Density Theory Study of the Mechanism of the [3 + 2] Cycloaddition Reaction. *Chemistry* **2023**, *5*, 2392–2405. <https://doi.org/10.3390/chemistry5040158>

Academic Editor: Maxim

L. Kuznetsov

Received: 30 September 2023

Revised: 25 October 2023

Accepted: 30 October 2023

Published: 6 November 2023



Copyright: © 2023 by the authors. Licensee MDPI, Basel, Switzerland. This article is an open access article distributed under the terms and conditions of the Creative Commons Attribution (CC BY) license (<https://creativecommons.org/licenses/by/4.0/>).

1. Introduction

Thiazolo[3,2-*a*] benzimidazole is an important heterocyclic privileged structure in medicinal chemistry possessing a wide range of biological activities. Thiazolo[3,2-*a*] benzimidazole is a fused bicyclic compound containing sulfur and nitrogen, which exist in nature, and synthetically inspired chemical structures with divergent medicinal targets and agrochemicals [1,2]. Several representative compounds incorporating this interesting scaffold have been shown to be anti-microbial and anti-cancer agents; such as compounds **I** and **II**, which exhibit anti-microbial activity [3–5]. Compound **I**, which has a trade name of Levamisole, is sold to fight and treat parasitic worm infections including ascariasis and hookworm infections, as shown in Figure 1. Compounds **III–IX** possess high efficacy halting different types of cancer cells with specific targets [6–10]; for example, compounds **III** and **VIII** target p53-MDM2 protein–protein interaction inhibitors as a target therapy for cancer treatment. Compound **IV** shows CXCR2 antagonists; on the other hand, compound **IX** exhibits carbonic anhydrase (CA IX) inhibitory activity as a promising target cancer therapy [11]. In 2021, Eldehna, W.M. et al. reported a set of compounds depending on the structure of the isatin lead compound with the thiazolo[3,2-*a*] benzimidazole scaffold,

obtaining a novel and potential CDK2 inhibitor with in vitro apoptotic anti-proliferative activity. The most active candidates showed potential CDK2 inhibition with nano-molar reactivity up to 96.46 nM [12].

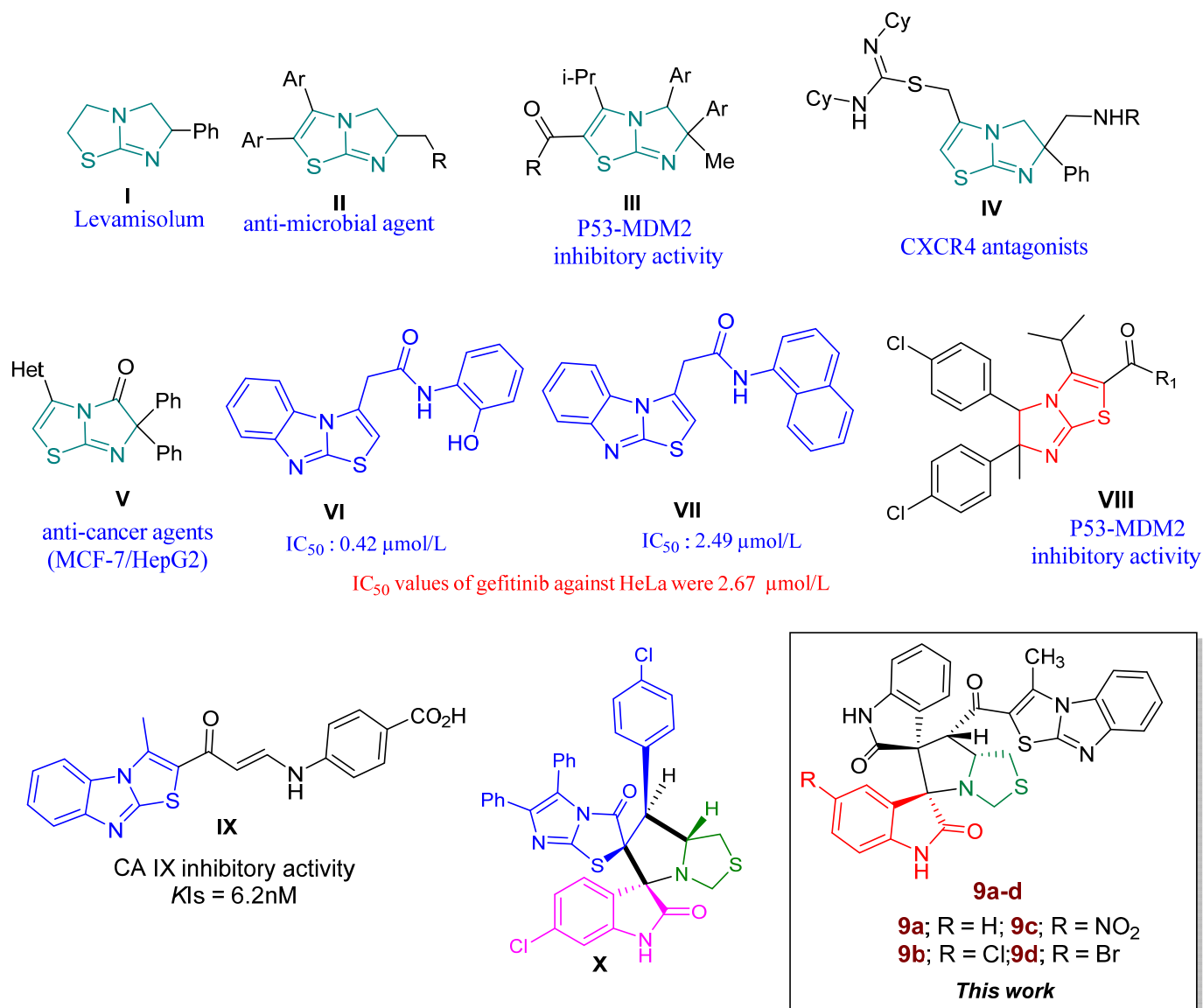


Figure 1. Representative examples of biologically active compounds having imidazothiazole.

Towards the development of an anti-microbial agent, Kamat et al. designed a new Schiff bases-based thiazolo[3,2-*a*] benzimidazole which possesses broad anti-microbial reactivity against gram-positive and gram-negative strains [13]. Many protein Kinase inhibitors for anti-cancer treatment have been designed and reported based on the annulation of the benzimidazole scaffold and between these targets' aurora kinase, CK2, CDK, FGFR, EGFR, and VEGFR-2 [14], in order to explore the chemistry of this interesting scaffold which has gained a lot of attention from chemists.

Barakat et al. are engaged in a research program to develop a new set of compounds based on spiro-heterocycles. In a recent study they constructed a new spirooxindole compound including a thiazolo[3,2-*a*] benzimidazole pharmacophore and studied its chemical reactivity (Compound X, Figure 1) [15]. Due to the variety of spiro-compounds, in particular spirooxindoles, they have a wide range of biological targets including anti-cancer, anti-inflammatory, diabetes, and others [16–20].

Based on the above findings, the aim of the present work was to prepare and study several new spiro-compounds based on thiazolo[3,2-*a*] benzimidazole via the [3 + 2] cycloaddition (32CA) reaction approach [15]. This procedure involves a one-pot multi-component synthesis that enables the formation of a diversity of highly complex molecules through an efficient, straightforward, and selective transformation.

The theoretical understanding of the key 32CA reaction step in these transformations is essential to guarantee more efficient future synthetic designs. In this sense, the Molecular Electron Density Theory (MEDT), ref. [21] based on the idea that changes in electron density but not molecular orbital interactions, are responsible for chemical reactivity, allows for a modern and rigorous new interpretation of organic chemical reactivity.

MEDT has allowed classifying 32CA reactions into four types depending on a general relationship found between the electronic structure and the reactivity of the participating three-atom-components (TACs) [22]. The proposed multicomponent process involves a series of azomethine ylides (AYs) **10a–d** generated in situ through the reaction between isatins **5a–d** and (*R*)-thiazolidine-4-carboxylic acid **8**. The simplest AYs are one of the most reactive species due to their *pseudodiradical* structure that enables them to participate in instant *pdr-type* 32CA reactions [23]. However, actual experimental substitution can change their parent *pseudodiradical* structure to less reactive *pseudo(mono)radical*, zwitterionic, or even carbenoid ones.

The purpose of the present work is to report the synthetic routes developed for the synthesis of novel spirooxindoles **9a–d** and the characterization of the molecular mechanism in order to understand the underlying factors responsible for the high reaction rate of the key 32CA reaction step.

2. Materials and Methods

Synthesis of 1*H*-benzo[*d*]imidazole-2-thiol **2**

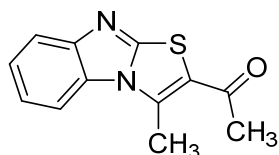
The synthesis of compound **2** is amended in the ESI.

Synthesis of compound (**3**) and acetyl derivative (**4**)

A mixture of (0.02 mol, 3 g) 1*H*-benzo[*d*]imidazole-2-thiol **2** and (0.02 mol, 2.80 g) of 3-chloro-2,4-pentanedione in 45 mL of 2-butanone was heated, in a 150 mL round bottom flask, under reflux for 5 h. The reaction mixture was cooled to room temperature. The resulting precipitate was filtered off, dried, and suspended in water. The water suspension was made basic with NaHCO₃ and obtained 4.63 g (93%) white solid of 3-((1*H*-benzo[*d*]imidazol-2-yl) thio)pentane-2,4-dione (**3**).

The product **3** (0.02 mol, 4.96 g) was refluxed in 60 mL of 5% HCl for 4 h. The reaction mixture was added to 400 mL of water and basified with aqueous sodium bicarbonate. The resulting solid was filtered off and dried to obtain 4.48 g (97%) of 1-(3-methylbenzo[4,5]imidazo[2,1-*b*]thiazol-2-yl)ethan-1-one (**4**).

1-(3-Methylbenzo[4,5]imidazo[2,1-*b*]thiazol-2-yl)ethan-1-one **4**

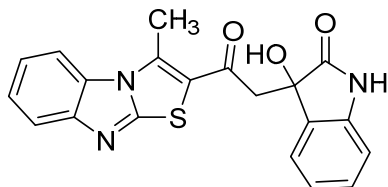


Yield (%): 97; White solid material; m.p.: 163–165 °C; Molecular Formula: C₁₂H₁₀N₂OS; [M⁺] m/z: 230; ¹H-NMR (500 MHz, DMSO-*d*₆) δ 8.01 (d, *J* = 8.2 Hz, 1H, Ar-H), 7.65 (d, *J* = 8.2 Hz, 1H, Ar-H), 7.36 (t, *J* = 8.3 Hz, 1H, Ar-H), 7.25 (t, *J* = 8.3 Hz, 1H, Ar-H), 3.03 (s, 3H, COCH₃), 2.56 (s, 3H, CH₃); ¹³C-NMR (126 MHz, DMSO-*d*₆) δ 191.6, 154.4, 148.8, 138.9, 130.9, 125.0, 123.6, 121.9, 119.2, 113.3, 30.1, 14.6; Anal. for C₁₂H₁₀N₂OS; calcd: C, 62.59; H, 4.38; N, 12.16 Found: C, 62.52; H, 4.30; N, 12.20

Synthesis of 3-hydroxy-3-(2-(3-methylbenzo[4,5]imidazo[2,1-*b*]thiazol-2-yl)-2-oxoethyl)indolin-2-one (**6**)

A mixture of acetyl derivative **4** (1.150 g, 5 mmol) and isatin **5a** (0.735 g, 5 mmol) in ethanol 20 mL and piperidine (0.15 mL) was stirred for 2 h, left overnight, and the obtained product was filtered.

3-Hydroxy-3-(2-(3-methylbenzo[4,5]imidazo[2,1-*b*]thiazol-2-yl)-2-oxoethyl)indolin-2-one **6**

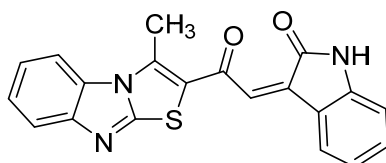


Yield (%): 96; Yellow solid material; m.p.: 243–245 °C; Molecular Formula: C₂₀H₁₅N₃O₃S; [M⁺] m/z: 377; IR (KBr, cm⁻¹): 3277 (OH), 1702–1668 (C=O), 1621 (C=N); ¹H-NMR (500 MHz, DMSO-*d*₆) δ 10.28 (s, 1H, NH), 8.00 (d, *J* = 8.2 Hz, 1H, ArH), 7.65 (d, *J* = 8.0 Hz, 1H, ArH), 7.40–7.33 (m, 1H, ArH), 7.32 (d, *J* = 7.4 Hz, 1H, ArH), 7.25 (t, *J* = 7.8 Hz, 1H, ArH), 7.15 (t, *J* = 8.4 Hz, 1H, ArH), 6.86 (t, *J* = 6.9 Hz, 1H, ArH), 6.79 (d, *J* = 7.9 Hz, 1H, ArH), 6.14 (s, 1H, OH), 3.88 (d, *J* = 17.1 Hz, 1H, CH₂), 3.54 (d, *J* = 17.1 Hz, 1H, CH₂), 3.02 (s, 3H, CH₃); ¹³C-NMR (126 MHz, DMSO-*d*₆) δ 190.3, 178.5, 154.2, 148.9, 143.4, 139.4, 132.0, 130.8, 129.6, 125.0, 124.3, 122.4, 122.0, 121.8, 119.3, 113.4, 110.1, 73.4, 49.0, 14.9; Anal. for C₂₀H₁₅N₃O₃S; calcd: C, 63.65; H, 4.01; N, 11.13 Found: C, 63.59; H, 4.06; N, 11.18.

Synthesis of 3-(2-(3-methylbenzo[4,5]imidazo[2,1-*b*]thiazol-2-yl)-2-oxoethylidene)indolin-2-one (**7**)

Compound **6** (1.51 g, 4 mmol) was refluxed with a mixture of glacial acetic acid (15 mL) and concentrated hydrochloric acid (3 mL) in an oil bath for 2 h. The reaction mixture was cooled to room temperature. A red compound was separated out which was filtered and recrystallized from ethanol to give red needles of compound (**7**).

3-(2-(3-methylbenzo[4,5]imidazo[2,1-*b*]thiazol-2-yl)-2-oxoethylidene)indolin-2-one **7**

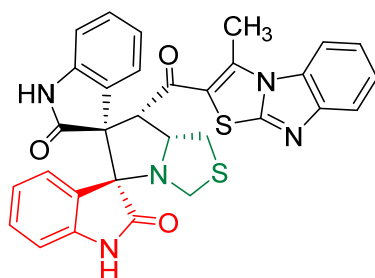


Yield (%): 88; Red solid material; m.p.: 255–257 °C; Molecular Formula: C₂₀H₁₃N₃O₂S; [M⁺] m/z: 359; IR (KBr, cm⁻¹): 3428 (NH), 1716–1653 (C=O), 1602 (C=N); ¹H-NMR (500 MHz, DMSO-*d*₆) δ 10.89 (s, 1H, N-H), 8.06 (d, *J* = 8.1 Hz, 1H, Ar-H), 8.00 (d, *J* = 7.6 Hz, 1H, Ar-H), 7.70 (d, *J* = 8.2 Hz, 1H, Ar-H), 7.43–7.37 (m, 2H, Ar-H, C-H), 7.30 (t, *J* = 8.4 Hz, 2H, Ar-H), 6.92 (t, *J* = 7.1 Hz, 1H, Ar-H), 6.84 (d, *J* = 7.8 Hz, 1H, Ar-H), 3.09 (s, 3H, CH₃); ¹³C-NMR (126 MHz, DMSO-*d*₆) δ 184.4, 168.51, 154.3, 147.6, 145.7, 140.8, 137.1, 133.9, 130.6, 127.4, 126.1, 125.6, 124.5, 122.5, 122.4, 120.2, 119.0, 113.8, 111.1, 15.4; Anal. for C₂₀H₁₃N₃O₂S; calcd: C, 66.84; H, 3.65; N, 11.69 Found: C, 66.79; H, 3.60; N, 11.74.

General procedure for synthesis of spiro compounds (**9a–d**)

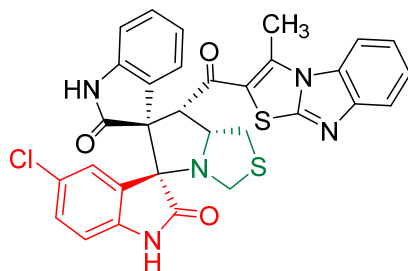
A mixture of the chalcone derivative **7** (0.5 mmol, 179.5 mg), isatin derivatives **5a–d** (0.5 mmol), and thiazolidine-4-carboxylic acid **8** (0.5 mmol, 66.5 mg) in ethanol (15 mL) was refluxed using an oil bath for an appropriate time, 8–10 h. After completion of the reaction TLC, the solvent volume was removed under vacuum. The crude was purified by column chromatography on silica gel (40% ethyl acetate in *n*-hexane) to produce the spiro compounds in a solid in pure form.

(3*S*,6'*R*,7'*S*)-7'-(3-Methylbenzo[4,5]imidazo[2,1-*b*]thiazole-2-carbonyl)-7',7*a*'-dihydro-1'*H*,3'*H*-dispiro[indoline-3,5'-pyrrolo[1,2-*c*]thiazole-6',3''-indoline]-2,2''-dione **9a**



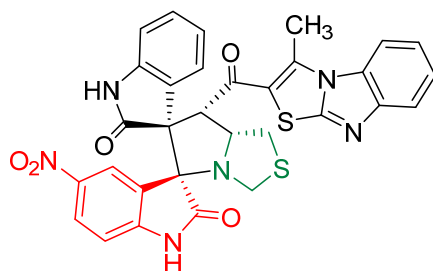
Yield (%): 78; White solid material; m.p.: 185–187 °C; Molecular Formula: $C_{31}H_{23}N_5O_3S_2$; $[M^+]$ m/z: 577; IR (KBr, cm^{-1}): 3416 (NH), 1721–1617 (C=O), 1572 (C=N); 1H -NMR (400 MHz, DMSO- d_6) δ 10.51 (s, 1H, N-H), 10.31 (s, 1H, N-H), 7.94 (d, J = 8.8 Hz, 1H, Ar-H), 7.63 (d, J = 8.1 Hz, 1H, Ar-H), 7.48 (d, J = 7.3 Hz, 1H, Ar-H), 7.37 (t, J = 7.7 Hz, 1H, Ar-H), 7.32 (d, J = 5.1 Hz, 1H, Ar-H), 7.26 (t, J = 7.7 Hz, 1H, Ar-H), 7.14 (d, J = 8.8 Hz, 1H, Ar-H), 6.96 (t, J = 7.7 Hz, 1H, Ar-H), 6.82 (d, J = 8.1 Hz, 1H, Ar-H), 6.72 (t, J = 7.7 Hz, 1H, Ar-H), 6.56 (d, J = 7.3 Hz, 1H, Ar-H), 6.34 (d, J = 8.1 Hz, 1H, Ar-H), 5.62–5.50 (m, 1H, C-H), 4.00 (d, J = 8.1 Hz, 1H, C-H $_{\alpha}$), 3.79 (d, J = 5.9 Hz, 1H, CH $_2$), 3.45 (d, J = 5.4 Hz, 1H, CH $_2$), 3.12–3.04 (m, 1H, CH $_2$), 2.93 (d, J = 6.6 Hz, 1H, CH $_2$), 2.87 (s, 3H, CH $_3$); ^{13}C -NMR (101 MHz, DMSO- d_6) δ 190.0, 179.2, 175.5, 153.5, 148.9, 143.1, 142.8, 138.7, 128.6, 127.5, 127.2, 127.0, 124.9, 124.4, 124.0, 122.3, 122.1, 121.8, 120.4, 119.3, 113.3, 109.8, 109.34, 74.5, 67.3, 63.0, 57.9, 45.7, 32.3, 14.9; Anal. for $C_{31}H_{23}N_5O_3S_2$; calcd: C, 64.45; H, 4.01; N, 12.12 Found: C, 64.49; H, 4.06; N, 12.15.

(3*S*,6'*R*,7'*S*)-5-Chloro-7'-(3-methylbenzo[4,5]imidazo[2,1-*b*]thiazole-2-carbonyl)-7',7*a*'-dihydro-1'*H*,3'*H*-dispiro[indoline-3,5'-pyrrolo[1,2-*c*]thiazole-6',3''-indoline]-2,2''-dione **9b**



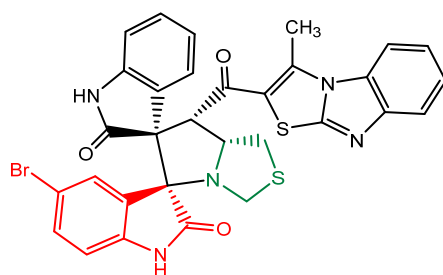
Yield (%): 75; White solid material; m.p.: 188–189 °C; Molecular Formula: $C_{31}H_{22}ClN_5O_3S_2$; $[M^+]$ m/z: 612; IR (KBr, cm^{-1}): 3412 (NH), 1725–1619 (C=O), 1567 (C=N); 1H -NMR (400 MHz, DMSO- d_6) δ 10.80 (s, 1H, N-H), 10.21 (s, 1H, N-H), 8.03 (d, J = 8.1 Hz, 1H, Ar-H), 7.75 (d, J = 8.1 Hz, 2H, Ar-H), 7.34 (d, J = 8.1 Hz, 1H, Ar-H), 7.28 (s, 1H, Ar-H), 7.26 (d, J = 5.9 Hz, 1H, Ar-H), 7.19 (t, J = 7.3 Hz, 2H, Ar-H), 7.11 (d, J = 5.9 Hz, 1H, Ar-H), 6.71 (d, J = 8.1 Hz, 1H, Ar-H), 6.57 (d, J = 7.3 Hz, 1H, Ar-H), 5.19 (d, J = 6.6 Hz, 1H, C-H $_{\alpha}$), 5.01–4.94 (m, 1H, C-H), 3.89 (d, J = 8.8 Hz, 1H, CH $_2$), 3.37 (d, J = 8.6 Hz, 1H, CH $_2$), 3.14 (dd, J = 10.3, 5.9 Hz, 2H, CH $_2$), 2.56 (s, 3H, CH $_3$); ^{13}C -NMR (101 MHz, DMSO- d_6) δ 190.1, 176.3, 171.2, 154.4, 149.1, 142.3, 128.9, 127.4, 125.6, 125.4, 120.1, 114.8, 108.5, 96.9, 75.8, 68.2, 14.2; Anal. for $C_{31}H_{22}ClN_5O_3S_2$; calcd: C, 60.83; H, 3.62; N, 11.44 Found: C, 60.89; H, 3.56; N, 11.39.

(3*S*,6'*R*,7'*S*)-7'-(3-Methylbenzo[4,5]imidazo[2,1-*b*]thiazole-2-carbonyl)-5-nitro-7',7*a*'-dihydro-1'*H*,3'*H*-dispiro[indoline-3,5'-pyrrolo[1,2-*c*]thiazole-6',3''-indoline]-2,2''-dione **9c**



Yield (%): 76; White solid material; m.p.: 182–184 °C; Molecular Formula: $C_{31}H_{22}N_6O_5S_2$; $[M^+]$ m/z: 622; IR (KBr, cm^{-1}): 3415 (NH), 1724–1616 (C=O), 1568 (C=N); 1H -NMR (400 MHz, DMSO- d_6) δ 11.03 (s, 1H, N-H), 10.68 (s, 1H, N-H), 8.36 (d, $J = 2.9$ Hz, 1H, Ar-H), 7.92 (d, $J = 8.1$ Hz, 1H, Ar-H), 7.62 (d, $J = 8.1$ Hz, 1H, Ar-H), 7.40–7.28 (m, 2H, Ar-H), 7.24 (t, $J = 8.1$ Hz, 1H, Ar-H), 7.14 (d, $J = 8.1$ Hz, 1H, Ar-H), 6.89 (t, $J = 7.7$ Hz, 1H, Ar-H), 6.83–6.74 (m, 2H, Ar-H), 6.39 (d, $J = 8.1$ Hz, 1H, Ar-H), 5.51–5.41 (m, 1H, C-H), 4.08 (d, $J = 8.8$ Hz, 1H, C-H $_{\alpha}$), 3.75 (d, $J = 5.9$ Hz, 1H, CH $_2$), 3.49 (d, $J = 5.9$ Hz, 1H, CH $_2$), 3.11 (dt, $J = 10.3, 5.5$ Hz, 1H, CH $_2$), 2.97 (t, $J = 8.8$ Hz, 1H, CH $_2$), 2.85 (s, 3H, CH $_3$); ^{13}C -NMR (101 MHz, DMSO- d_6) δ 189.8, 178.3, 175.8, 153.7, 149.8, 148.7, 143.1, 142.7, 142.5, 138.8, 130.3, 130.1, 128.6, 128.0, 125.2, 124.9, 123.8, 123.2, 122.1, 121.7, 120.3, 119.3, 113.4, 110.5, 109.8, 73.7, 67.6, 57.6, 45.9, 32.3, 14.2; Anal. for $C_{31}H_{22}N_6O_5S_2$; calcd: C, 59.80; H, 3.56; N, 13.50 Found: C, 59.87; H, 3.61; N, 13.56.

(3*S*,6'*R*,7'*S*)-5-Bromo-7'-(3-methylbenzo[4,5]imidazo[2,1-*b*]thiazole-2-carbonyl)-7',7*a*'-dihydro-1'*H*,3'*H*-dispiro[indoline-3,5'-pyrrolo[1,2-*c*]thiazole-6',3''-indoline]-2,2''-dione **9d**



Yield (%): 81; Pale yellow solid material; m.p.: 186–188 °C; Molecular Formula: $C_{31}H_{22}BrN_5O_3S_2$; $[M^+]$ m/z: 655; IR (KBr, cm^{-1}): 3414 (NH), 1724–1618 (C=O), 1569 (C=N); 1H -NMR (400 MHz, DMSO- d_6) δ 10.47 (s, 1H, N-H), 10.18 (s, 1H, N-H), 8.00 (d, $J = 8.8$ Hz, 1H, Ar-H), 7.76 (d, $J = 7.3$ Hz, 2H, Ar-H), 7.57 (s, 1H, Ar-H), 7.42 (d, $J = 7.3$ Hz, 2H, Ar-H), 7.19 (t, $J = 7.3$ Hz, 2H, Ar-H), 7.13 (d, $J = 8.1$ Hz, 1H, Ar-H), 6.65 (d, $J = 8.1$ Hz, 1H, Ar-H), 6.38 (d, $J = 8.1$ Hz, 1H, Ar-H), 5.19 (d, $J = 7.3$ Hz, 1H, C-H $_{\alpha}$), 5.04–4.94 (m, 1H), 3.89 (d, $J = 8.1$ Hz, 1H), 3.69 (d, $J = 5.9$ Hz, 1H), 3.19–3.10 (m, 2H), 2.60 (s, 3H, CH $_3$); ^{13}C -NMR (101 MHz, DMSO- d_6) δ 189.0, 178.8, 175.0, 153.5, 149.3, 142.7, 137.7, 133.7, 130.2, 126.4, 124.0, 122.3, 122.2, 118.7, 113.0, 73.7, 67.5, 60.1, 30.8, 13.0; Anal. for $C_{31}H_{22}BrN_5O_3S_2$; calcd: C, 56.71; H, 3.38; N, 10.67 Found: C, 56.75; H, 3.34; N, 10.71.

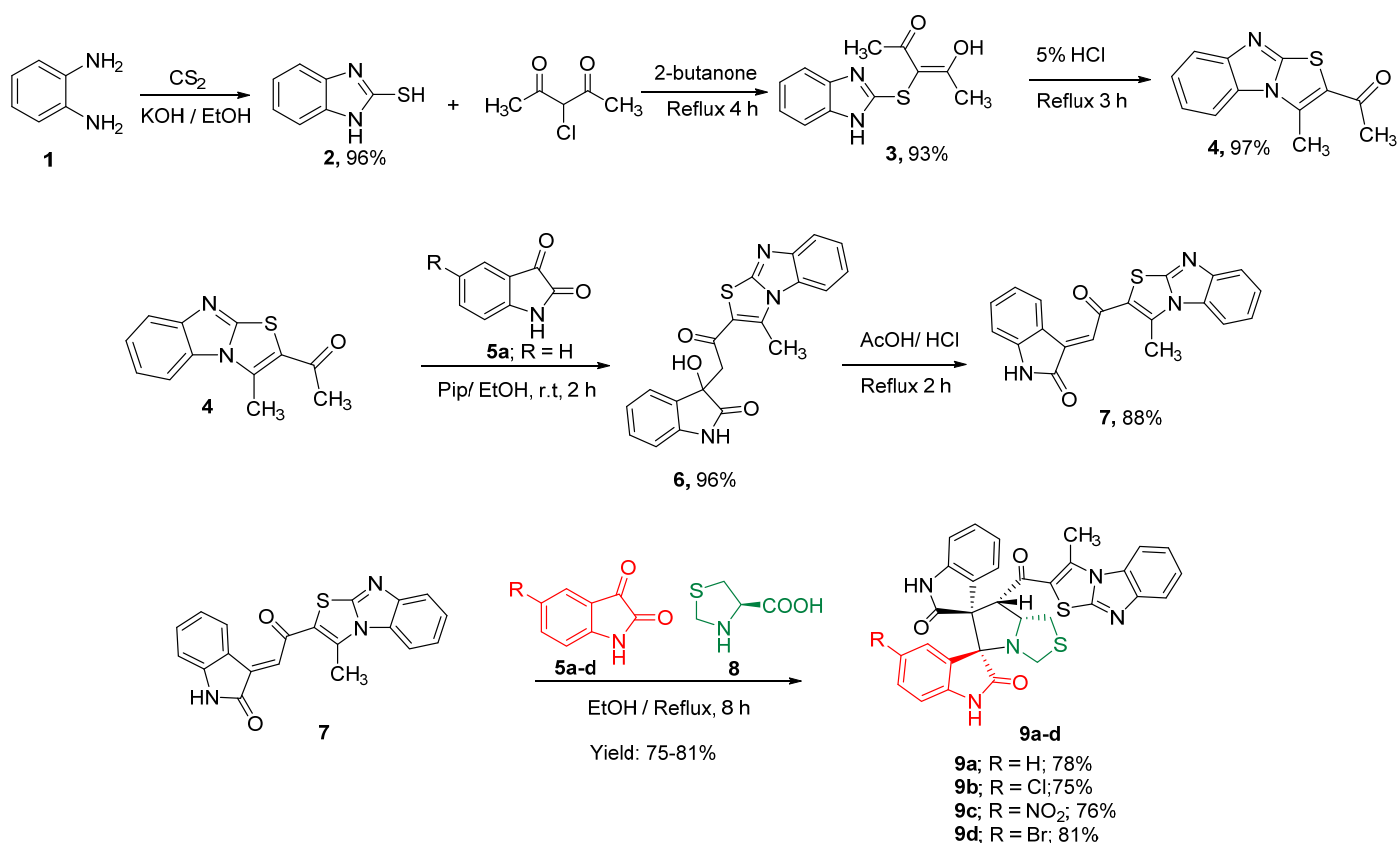
3. Results and Discussion

3.1. Synthesis of Spiro Compounds (9a–d)

Nitrogen- and sulfur-containing heterocycles are common substructures in a wide range of biologically active natural products and pharmaceutical small molecules. Some of the most important ones are imidazo[2,1-*b*]thiazole derivatives because of their diverse biological activities. In this work, as a last example of the synthesis of new spiro-derivatives, an attempt is made to synthesize a novel series of spiro compounds grafted with imidazo[2,1-*b*]thiazole scaffold, as depicted in Scheme 1.

3.1.1. Synthesis of Acetyl Derivative (4)

In the present work, 2-mercaptobenzimidazole **2** was synthesized via the reaction of *o*-phenylenediamine with carbon disulfide using the reflux method and the presence of an equivalent amount of potassium hydroxide in a mixture of ethanol and water as a solvent. Compound **3** was synthesized via the reaction of compound **2** with 3-chloroacetylacetone using 2-butanone as a solvent. The acetyl derivative **4** was synthesized via a condensation reaction of compound **3** in 5% HCl for 3 h. The prepared compounds were characterized on the basis of their elemental analysis as well as 1H -NMR, ^{13}C -NMR, and IR spectroscopy.



Scheme 1. Synthesis of spiro compounds (**9a–d**).

3.1.2. Synthesis of Spiro Compounds (**9a–d**)

To synthesize the targeted spiro compounds, three synthetic routes were outlined in Scheme 1. The first step in this synthesis involved crossed aldol condensation between the acetyl derivative **4** with the isatin in a basic medium using piperidine to give the aldol product **6** which then dehydrated easily in the second step by using acetic acid with drops of hydrochloric acid, to yield the expected α,β -unsaturated carbonyl compound **7**. The final step, the multicomponent reaction, was carried out using a mixture of isatin derivatives **5a–d** with (*R*)-thiazolidine-4-carboxylic acid **8** in ethanol followed by the addition of an equivalent amount of chalcone **7**. The reaction proceeds through decarboxylative condensation of isatin with (*R*)-thiazolidine-4-carboxylic acid to generate an azomethine ylide **10a–d**. The generated TAC subsequently undergoes 32CA reaction with the chalcone **7** to afford novel dispiro-oxindolopyrrolizidines **9a–d**. The prepared compounds were characterized on the basis of their elemental analysis as well as ¹H-NMR, ¹³C-NMR, and IR spectroscopy. In all cases the TLC of the product showed the presence of one single spot referring to only one product. Similarly, the proposed structures of aldol product **6** and α,β -unsaturated carbonyl compound **7** were confirmed by the same spectroscopic analysis tools. The IR spectrum of **6** showed peaks at 3277 cm⁻¹ for the O-H group and 1702 cm⁻¹ due to the oxindole ring carbonyl whilst the benzoyl carbonyl appeared at 1668 cm⁻¹ (see Supplementary Materials). The ¹H-NMR spectrum of **6** exhibited the NH proton at δ 10.28 ppm, the aromatic protons in the region of δ 8.01–6.78 ppm, and the O-H proton at δ 6.14 ppm (see Supplementary Materials). The ¹³C-NMR spectrum of the proposed carbon atoms is perfectly shown in the supplementary materials. The IR spectrum of compound **7** revealed two strong absorption bands at 1716 and 1653 cm⁻¹ due to two carbonyl groups, and revealed the absence of a band corresponding to the OH group and the appearance of an absorption band for the NH group at 3428 cm⁻¹ (see Supplementary Materials). Comparative analysis of the ¹H-NMR spectrum of compound **7** confirms my interpretation because the elimination of the OH-group proton via the dehydration reaction led to an

extinction peak for the O-H group in compound **7** and the appearance of the signal at 7.39 ppm for the CH_(α) proton (see supplementary materials) from the ¹³C-NMR spectrum. The structures of the desired spiro compounds **9a–d** were deduced by the IR and ¹H-NMR spectrum, for example, The IR spectrum of compound **9c**, taken as a typical example of the prepared series, revealed two strong absorption bands at 1724 and 1616 cm⁻¹ due to two carbonyl groups, and the appearance of an absorption band for the NH group at 3415 cm⁻¹ (see supplementary materials). The ¹H-NMR spectrum of compound **9c** displayed two singlet's signals at δ 11.03 and 10.68 ppm, assignable to two N-H group, and the aromatic protons in the region of δ 8.37–6.38 ppm (see Supplementary Materials). The ¹³C-NMR spectrum of the proposed carbon atoms is perfectly shown in the Supplementary Materials, which appeared three peaks for carbonyl groups at 189, 178, and 175 ppm.

3.2. MEDT Study of the 32CA Reaction between AY **10a** and Chalcone **7**

A theoretical MEDT [21] study was conducted to comprehend the experimental formation of spiro compounds **9a–d** through the final 32CA reaction step of the reported process (see Scheme 1). To do so, the 32CA reaction of chalcone **7** with the simplest AY **10a**, generated in situ through the reaction between isatin **5a** and (*R*)-thiazolidine-4-carboxylic acid **8**, was theoretically investigated as the reference prototype.

3.2.1. Analysis of Reactivity Indicators

The reactivity indices [22,24] offer valuable insights into predicting and understanding reactivity in polar reactions [25]. Table 1 presents the global reactivity indices, such as the electronic chemical potential μ, chemical hardness η, electrophilicity ω, and nucleophilicity *N*, for both AY **10a** and chalcone **7**.

Table 1. ωB97X-D/6-311G(d,p) gas-phase electronic chemical potential μ, chemical hardness η, electrophilicity ω and nucleophilicity *N* indices, in eV, of AY **10a**, and chalcone **7**.

	μ	η	ω	<i>N</i>
Chalcone 7	−4.61	6.45	1.65	3.56
AY 10a	−3.29	6.83	0.79	4.70

Comparing the electronic chemical potentials, μ [26], of AY **10a** and chalcone **7** reveals a notable difference, with AY **10a** having a higher value, −3.29 eV, compared to chalcone **7**, −4.61 eV. This difference indicates that, in a polar 32CA reaction, there will be a global electron density transfer (GEDT) [27] from AY **10a** to chalcone **7**. Therefore, AY **10a** plays the role of the nucleophile, while chalcone **7** takes on the role of the electrophile, leading to the classification of the corresponding 32CA reaction as a forward electron density flux (FEDF) process [28].

Delving further into the properties of AY **10a**, its electrophilicity ω index [29] is 0.79 eV, placing it in the category of a moderate electrophile according to the electrophilicity scale [24,30]. Additionally, it exhibits a nucleophilicity *N* index [31] of 4.70 eV, signifying its classification as a strong nucleophile based on the nucleophilicity scale [24,30]. In fact, its nucleophilic character exceeds 4.0 eV, being classified as a supernucleophile [25,30]. On the other hand, chalcone **7** presents electrophilicity ω and nucleophilicity *N* indices of 1.65 eV and 3.56 eV, respectively, indicating its status as both a strong electrophile and a strong nucleophile.

Considering the supernucleophilic character of AY **10a** and the strong electrophilic character of chalcone **7**, it can be inferred that the corresponding FEDF 32CA reaction will possess a high polar character [25]. This high polarity enhances reaction rates by reducing activation energies, primarily due to more favorable nucleophilic/electrophilic interactions that effectively stabilize the electrophile [27].

Chalcone **7** presents several susceptible sites for the nucleophilic addition of AY **10a**. In particular, α,β-unsaturated carbonylic compounds such as chalcones can experience

cycloaddition at the conjugated C4–C5 double bond or at the C6–O7 carbonyl group. In order to rule out unlikely reaction paths, the electrophilic P_k^+ Parr functions [32] at chalcone 7 were analyzed (see Figure 2).

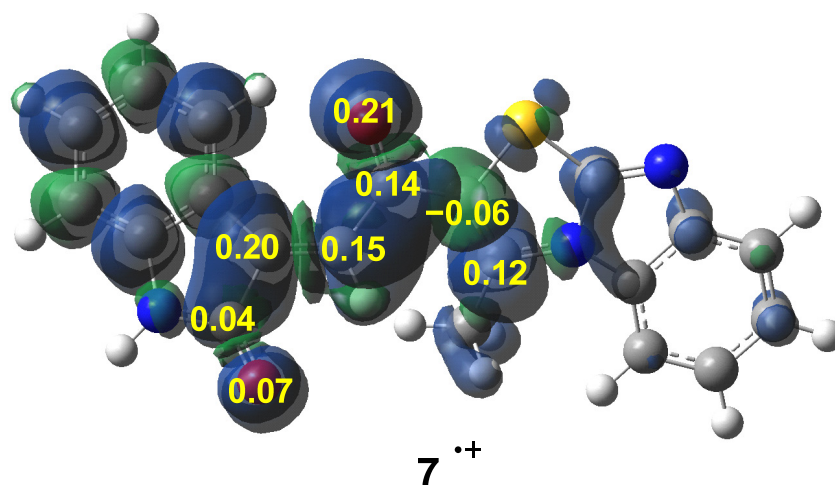


Figure 2. 3D representation of the Mulliken atomic spin densities of the radical anion of chalcone 7, together with the electrophilic P_k^+ Parr functions of chalcone 7 at the most relevant centers.

Analysis of the electrophilic P_k^+ Parr functions at chalcone 7 shows that the ethylene C4–C5 double bond and carbonyl C6–O7 group that constitute the central α,β -unsaturated carbonyl core of chalcone 7 are the two most electrophilically activated regions, with an average value of $P_k^+ = 0.35$ each one. Note that the benzimidazole carbonyl and the benzimidazothiazole regions are not sufficiently activated electrophilically (see Figure 2). Consequently, only two chemoisomeric paths involving the 32CA reaction on C4–C5 and C6–O7 will be considered.

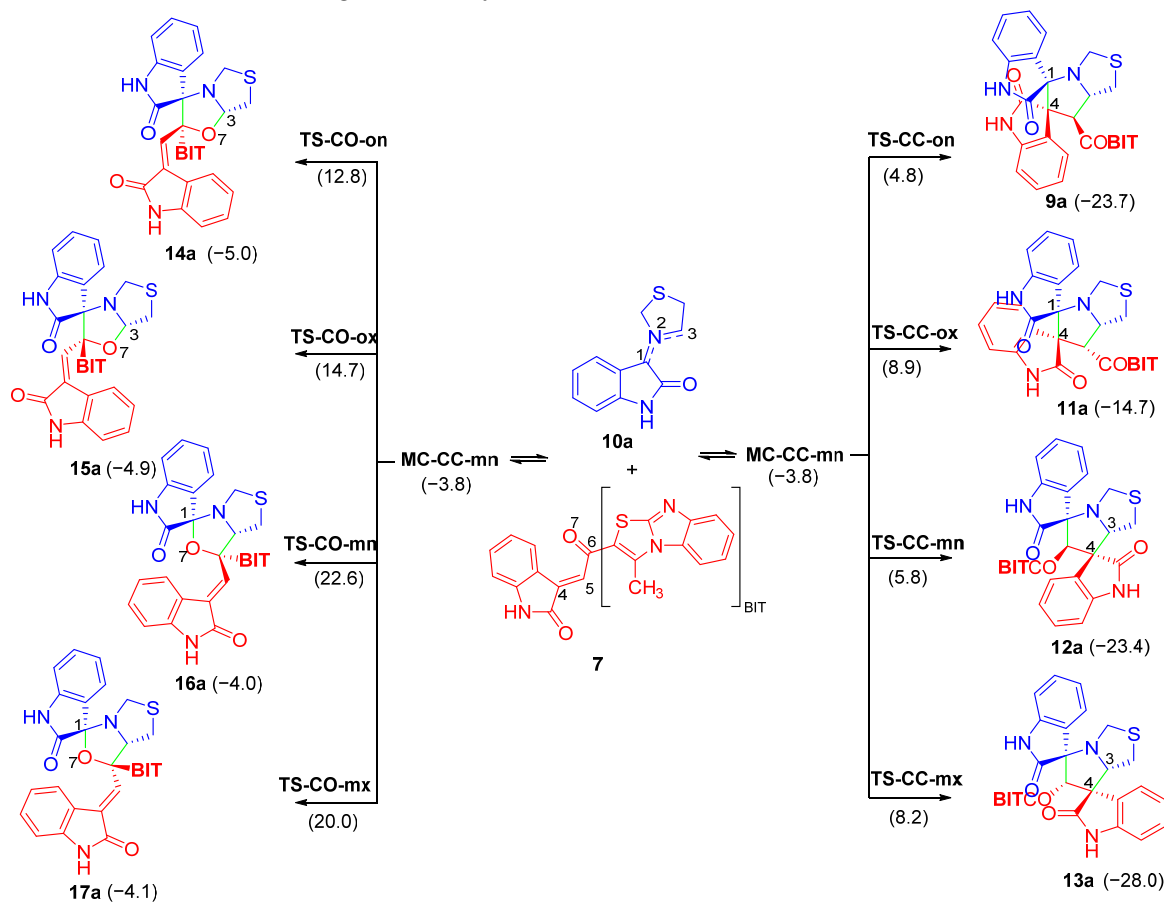
3.2.2. Study of the Competitive Reaction Paths

Due to the non-symmetry of the reagents, the corresponding 32CA reaction of AY 10a on the main α,β -unsaturated carbonyl core of chalcone 7 can take place along two *ortho/meta* regioisomeric and two *endo/exo* stereoisomeric approach modes for each chemoisomeric path, thus leading to a total of eight competitive reaction paths (see Scheme 2). Relative Gibbs free energies of the characterized stationary points are given in Scheme 2, the Gibbs free energy profiles associated with the eight competitive reaction paths are represented in Figure 3, and full thermodynamic data are given in Table S1 in the Supplementary Materials.

Thorough examination of the eight reaction paths shows that the 32CA reaction proceeds via a one-step mechanism. Each path involves the formation of a stable molecular complex (MC), brought about by weak intermolecular interactions between the reagents. However, due to thermodynamic equilibrium among all of them, only the most stable complex, **MC-CC-mn**, was selected as the energy reference. Formation of **MC-CC-mn** is slightly exergonic, releasing $3.8 \text{ kcal}\cdot\text{mol}^{-1}$ (see Figure 3).

Taking into account the formation of **MC-CC-mn**, the activation Gibbs free energies for the competitive isomeric reaction paths range from 8.6 (**TS-CC-on**) to 12.7 (**TS-CC-ox**) $\text{kcal}\cdot\text{mol}^{-1}$ for the addition on the C4–C5 double bond, and from 16.6 (**TS-CO-on**) to 26.4 (**TS-CO-mn**) $\text{kcal}\cdot\text{mol}^{-1}$ for the addition on the carbonyl C6–O7 bond. The reactive *pseudo(mono)radical* structure previously characterized [33] for AY 10a contributes to these low activation barriers. Furthermore, while the chemoisomeric C4–C5 reaction paths are highly exergonic, from 28.0 (**13a**) to 14.7 (**11a**) $\text{kcal}\cdot\text{mol}^{-1}$, rendering the corresponding addition on the C4–C5 double bond irreversible under the reaction conditions, the C6–O7 reaction paths are only slightly exergonic, from 5.0 (**14a**) to 4.0 (**16a**), making the corresponding addition on the C6–O7 bond reversible. Consequently, the 32CA reaction involving the C4–C5 double

bond of chalcone **7** is clearly favored both kinetically and thermodynamically over the one involving the carbonyl C6–O7 bond.



Scheme 2. Studied competitive reaction paths associated with the 32CA reaction of AY **10a** with chalcone **7**. ω B97X-D/6-311G(d,p) relative Gibbs free energies, in ethanol at 78 °C, are given in parentheses with respect to the separated reagents, in kcal·mol⁻¹.

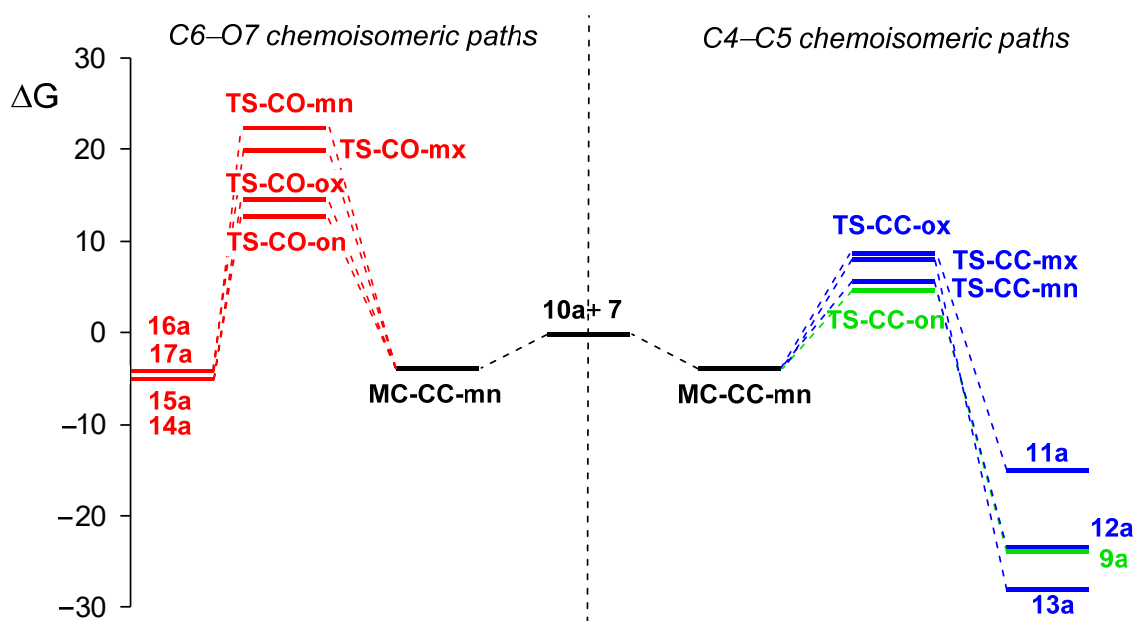


Figure 3. ω B97X-D/6-311G(d,p) Gibbs free energy profile, in kcal·mol⁻¹, in ethanol at 78 °C, for the competitive reaction paths associated with the 32CA reaction of AY **10a** with chalcone **7**.

Due to the irreversibility of the more favorable chemoisomeric C4–C5 reaction paths, the product distribution is kinetically controlled. Utilizing the Eyring–Polanyi kinetics equation [34], the predicted product distribution is 81.1% (**9a**), 0.2% (**11a**), 18.0% (**12a**), and 0.6% (**13a**); no cycloadduct from the 32CA reaction on the C6–O7 carbonyl is expected, based on the 0.0% obtained for **14a–17a**. These results indicate absolute C4–C5 chemoselectivity, complete *endo* stereoselectivity, and high *ortho* regioselectivity, leading to the formation of spirooxindole **9a** as the main product through **TS-CC-on**, which aligns precisely with the experimental data (see Scheme 1).

Figure 4 displays the optimized geometries of the four isomeric transition state structures (TSs) associated with the more favorable 32CA reaction on the C4–C5 double bond in ethanol. The C–C distances between the interacting carbons reveal that, while the *ortho* regioisomeric TSs are related with highly asynchronous bond formation processes, the *meta* TSs are rather synchronous, especially **TS-CC-mn** with a $\Delta l = 0.02$ Å (see Figure 4). With the exception of synchronous **TS-CC-mn**, the shorter C–C distance in the other three TSs involves the C3 carbon of the thiazole ring of AY **10a**. Similarly, except for **TS-CC-mx**, formation at the C5 carbon of chalcone **7** is more advanced. This implies that at the more favorable *ortho* regioisomeric reaction paths, the preferred two-center interaction is that between the C3 and C5 carbons. The most stable **TS-CC-on**, characterized by C3–C5 and C1–C4 distances of 2.186 and 2.688 Å, respectively, shows the highest degree of asynchronicity, though it is very similar to **TS-CC-ox**. Examining the intrinsic reaction coordinate (IRC) path [35] from the most favorable **TS-CC-on** to **9a** reveals that the 32CA reaction indeed follows a non-concerted *two-stage one-step* mechanism [36], characterized by complete formation of the first C3–C5 single bond before initiating the formation of the second C1–C4 single bond (see Figure S20 in Supplementary Materials).

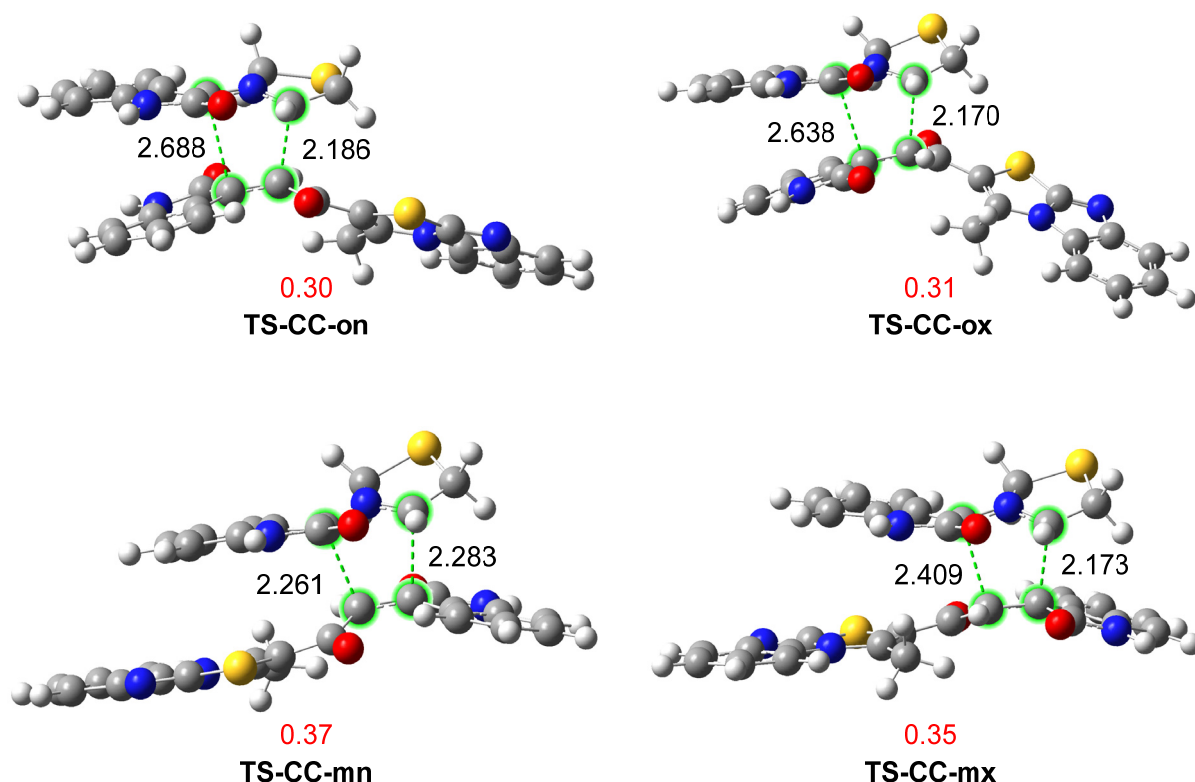


Figure 4. ω B97X-D/6-311G(d,p) optimized geometries in ethanol of the TSs involved in the more favorable C4–C5 chemoisomeric reaction paths of the 32CA reaction between AY **10a** with chalcone **7**. Distances are given in angstroms, Å, while GEDT values, in red, are given in average number of electrons, e.

Figure 4 also includes the GEDT [27] values for the four isomeric TSs associated with the 32CA reaction on the C4–C5 double bond. The GEDT at the TS serves as a measure of the polar character of the 32CA reaction. GEDT values below 0.05 e indicate non-polar processes, while values above 0.20 e indicate highly polar processes. The most favorable **TS-CC-on** presents a GEDT value of 0.30 e. This high value is attributed to the supernucleophilic nature of AY **10a** and the strong electrophilic character of chalcone **7** (refer to Table 1). Consequently, the 32CA reaction through **TS-CC-on** possesses a remarkable polar character, which accounts for its low activation Gibbs free energy of 8.6 kcal·mol⁻¹ and the observed total *endo* stereoselectivity. Note that polar cycloaddition reactions are typically *endo* stereoselective. Furthermore, the positive sign of the GEDT computed at the AY framework of the TS indicates an electron density flux from AY **10a** to chalcone **7**, classifying this 32CA reaction as FEDF [28], in line with the previous analysis of the reactivity indices.

4. Conclusions

A novel series of dispiro-oxindolopyrrolizidines analogs were synthesized with incorporation of a thiazolo[3,2-*a*] benzimidazole scaffold via a 32CA reaction approach in one-pot multi-component reaction. The desired novel dispiro-oxindolopyrrolizidines **9a–d** was obtained in high chemical yield, in a stereoselective fashion with four stereogenic centers.

An MEDT study of the key 32CA reaction step between the simplest in situ generated AY **10a** and chalcone **7** was performed at the ω B97xD/6-311g(d,p) computational level in order to characterize the molecular mechanism and understand the experimental outcomes. Among the eight possible isomeric reaction paths, the *ortho/endo* reaction path leading to spiro-compound **9a** is the most favorable one, explaining the experimentally observed high selectivity with a computed regioisomeric product distribution ratio of ca. 80:20. Analysis of the geometrical parameters at the TSs reveals a non-concerted *two-stage one-step* mechanism with complete formation of the first C3–C5 single bond before initiating the formation of the second C1–C4 single bond. Finally, the very high polar character of the reaction is a consequence of the high supernucleophilic character of AY **10a** and the strong electrophilic character of chalcone **7**. Thus, both the reactive *pseudo(mono)radical* electronic structure of the generated AYs and the high polar character of the corresponding *pnr-type* 32CA reactions account for the low computed activation Gibbs free energies and total *endo* stereoselectivities of this exergonic reaction.

The present study adds new compounds to the valuable family of bioactive thiazolo[3,2-*a*] benzimidazole-embodied dispiro-oxindolopyrrolizidines, and provides a comprehensive MEDT study of their formation via the key 32CA reaction that helps us understanding the high reaction rates and selectivities for future synthetic designs.

Supplementary Materials: The following supporting information can be downloaded at: <https://www.mdpi.com/article/10.3390/chemistry5040158/s1>, Figure S1: 1H-NMR Spectrum of compound (2); Figure S2: 13C-NMR Spectrum of compound (2); Figure S3: 1H-NMR Spectrum of compound (4); Figure S4: 13C-NMR Spectrum of compound (4); Figure S5: IR Spectrum of compound (6); Figure S6: 1H-NMR Spectrum of compound (6); Figure S7: 13C-NMR Spectrum of compound (6); Figure S8: IR Spectrum of compound (7); Figure S9: 1H-NMR Spectrum of compound (7); Figure S10: 13C-NMR Spectrum of compound (7); Figure S11: 1H-NMR Spectrum of compound (9a); Figure S12: 13C-NMR Spectrum of compound (9a); Figure S13: 1H-NMR Spectrum of compound (9b); Figure S14: 13C-NMR Spectrum of compound (9b); Figure S15: IR Spectrum of compound (9c); Figure S16: 1H-NMR Spectrum of compound (9c); Figure S17: 13C-NMR Spectrum of compound (9c); Figure S18: 1H-NMR Spectrum of compound (9d); Figure S19: 13C-NMR Spectrum of compound (9d); Computational Protocol; Table S1: ω B97X-D/6-311G(d,p) enthalpies, entropies, and Gibbs free energies, and the relative ones with respect to the separated reagents, for the stationary points involved in the 32CA reaction of AY **10a** with chalcone **7**; Figure S20: ω B97X-D/6-311G(d,p) IRC path associated with the most favorable *ortho/endo* reaction path via **TS-CC-on** in ethanol; Cartesian coordinates and electronic energies of the stationary points involved in the 32CA reaction between AY **10a** and chalcone **7** in ethanol. Imaginary frequencies for TSs at 78 °C are included.

Author Contributions: Conceptualization, A.B.; methodology, S.A., A.S.A. and M.A.; software, M.R.-G.; validation, S.A., A.S.A. and M.R.-G.; formal analysis, S.A., A.S.A. and M.A.; investigation, S.A., A.S.A. and M.A.; resources, A.B.; data curation, A.B. and M.R.-G.; writing—original draft preparation, A.B. and M.R.-G.; writing—review and editing, A.B. and M.R.-G.; supervision, A.B. and A.M.A.-M.; funding acquisition, A.B. All authors have read and agreed to the published version of the manuscript.

Funding: The authors extend their appreciation to the Deputyship for Research and Innovation, “Ministry of Education” in Saudi Arabia for funding this research work through the project number IFKSUOR3–128-3. This work has also been supported by the Ministry of Science and Innovation (MICINN) of the Spanish Government, through the project PID2019-110776GB-I00 (AEI/FEDER, UE).

Data Availability Statement: Not applicable.

Acknowledgments: The authors extend their appreciation to the Deputyship for Research & Innovation, “Ministry of Education” in Saudi Arabia for funding this research work through the project number IFKSUOR3–128-3. Gratitude is also expressed to the Ministry of Science and Innovation (MICINN) of the Spanish Government, for the project PID2019-110776GB-I00 (AEI/FEDER, UE).

Conflicts of Interest: The authors declare no conflict of interest.

References

1. Li, J.J. *Heterocyclic Chemistry in Drug Discovery*; John Wiley & Sons, Inc.: Hoboken, NJ, USA, 2013.
2. Shareef, M.A.; Khan, I.; Babu, B.N.; Kamal, A. A Comprehensive review on the therapeutic versatility of imidazo[2,1-b]thiazoles. *Curr. Med. Chem.* **2020**, *27*, 6864–6887. [[CrossRef](#)] [[PubMed](#)]
3. Çapan, G.; Ulusoy, N.; Ergenç, N.; Kiraz, M. New 6-phenylimidazo[2,1-b]thiazole derivatives: Synthesis and antifungal activity. *Monatsh. Chem.* **1999**, *130*, 1399–1407. [[CrossRef](#)]
4. Cascioferro, S.; Parrino, B.; Petri, G.L.; Cusimano, M.G.; Schillaci, D.; DI Sarno, V.; Musella, S.; Giovannetti, E.; Cirrincione, G.; Diana, P. 2,6-Disubstituted imidazo[2,1-b][1,3,4]thiadiazole derivatives as potent staphylococcal biofilm inhibitors. *Eur. J. Med. Chem.* **2019**, *167*, 200–210. [[CrossRef](#)] [[PubMed](#)]
5. Li, Y.; Bionda, N.; Fleeman, R.; Wang, H.; Ozawa, A.; Houghten, R.A.; Shaw, L. Identification of 5,6-dihydroimidazo[2,1-b]thiazoles as a new class of antimicrobial agents. *Bioorg. Med. Chem.* **2016**, *24*, 5633–5638. [[CrossRef](#)] [[PubMed](#)]
6. Sbenati, R.M.; Semreen, M.H.; Semreen, A.M.; Shehata, M.K.; Alsaghir, F.M.; El-Gamal, M.I. Evaluation of imidazo[2,1-b]thiazole-based anticancer agents in one decade (2011–2020): Current status and future prospects. *Bioorg. Med. Chem.* **2021**, *29*, 115897. [[CrossRef](#)] [[PubMed](#)]
7. Başoğ lu, F.; Ulusoy-Güzeldemirci, N.; Akalın-Çiftçi, G.; Çetinkaya, S.; Ece, A. Novel imidazo[2,1-b] thiazole-based anticancer agents as potential focal adhesion kinase inhibitors: Synthesis, in silico, and in vitro evaluation. *Chem. Biol. Drug. Des.* **2021**, *98*, 270–282. [[CrossRef](#)]
8. Potikha, L.M.; Brovarets, V.S. Synthesis of imidazo[2,1-b][1,3] thiazoles—potential anticancer agents derived from γ -bromodiprones. *Chem. Heterocycl. Compd.* **2020**, *56*, 1073–1077. [[CrossRef](#)]
9. Miyazaki, M.; Naito, H.; Sugimoto, Y.; Kawato, H.; Okayama, T.; Shimizu, H.; Miyazaki, M.; Kitagawa, M.; Seki, T.; Fukutake, S.; et al. Lead optimization of novel p53-MDM2 interaction inhibitors possessing dihydroimidazothiazole scaffold. *Bioorg. Med. Chem. Lett.* **2013**, *23*, 728–732. [[CrossRef](#)]
10. Mona, C.E.; Besserer-Offroy, É.; Cabana, J.; Leduc, R.; Lavigne, P.; Heveker, N.; Marsault, É.; Escher, E. Design, synthesis, and biological evaluation of CXCR4 ligands. *Org. Biomol. Chem.* **2016**, *14*, 10298–10311. [[CrossRef](#)]
11. Alkhalidi, A.A.M.; Al-Sanea, M.M.; Nocentini, A.; Eldehna, W.M.; Elsayed, Z.M.; Bonardi, A.; Abo-Ashour, M.F.; El-Damasy, A.K.; Abdel-Maksoud, M.S.; Al-Warhi, T.; et al. 3-Methylthiazolo[3,2-a] benzimidazole-benzenesulfonamide conjugates as novel carbonic anhydrase inhibitors endowed with anticancer activity: Design, synthesis, biological and molecular modeling studies. *Eur. J. Med. Chem.* **2020**, *207*, 112745. [[CrossRef](#)]
12. Eldehna, W.M.; El Hassab, M.A.; Abo-Ashour, M.F.; Al-Warhi, T.; Elaasser, M.M.; Safwat, N.A.; Suliman, H.; Ahmed, M.F.; Al-Rashood, S.T.; Abdel-Aziz, H.A.; et al. Development of isatin-thiazolo[3,2-a] benzimidazole hybrids as novel CDK2 inhibitors with potent in vitro apoptotic anti-proliferative activity: Synthesis, biological and molecular dynamics investigations. *Bioorg. Chem.* **2021**, *110*, 104748. [[CrossRef](#)] [[PubMed](#)]
13. Kamat, V.; Yallur, B.C.; Poojary, B.; Patil, V.B.; Nayak, S.P.; Krishna, P.M.; Joshi, S.D. Synthesis, molecular docking, antibacterial, and anti-inflammatory activities of benzimidazole-containing tricyclic systems. *J. Chin. Chem. Soc.* **2021**, *68*, 1055–1066. [[CrossRef](#)]
14. Ali, A.M.; Tawfik, S.S.; Mostafa, A.S.; Massoud, M.A.M. Benzimidazole-based protein kinase inhibitors: Current perspectives in targeted cancer therapy. *Chem. Biol. Drug Des.* **2022**, *100*, 656–673. [[CrossRef](#)] [[PubMed](#)]
15. Altowyan, M.S.; Soliman, S.M.; Haukka, M.; Al-Shaalan, N.H.; Alkharboush, A.A.; Barakat, A. [3+2] Cycloaddition Reaction for the Stereoselective Synthesis of a New Spirooxindole Compound Grafted Imidazo[2,1-b]thiazole Scaffold: Crystal Structure and Computational Study. *Crystals* **2022**, *12*, 5. [[CrossRef](#)]

16. Barakat, A.; Islam, M.S.; Ghawas, H.M.; Al-Majid, A.M.; Elsenduny, F.; Badria, F.A.; Elshaier, Y.; Ghabbour, H.A. Design and synthesis of new substituted spirooxindoles as potential inhibitors of the MDM2–p53 interaction. *Bioorg. Chem.* **2019**, *86*, 598–608. [[CrossRef](#)]
17. Altowyan, M.S.; Barakat, A.; Al-Majid, A.M.; Al-Ghulikah, H. Spiroindolone analogues bearing benzofuran moiety as a selective cyclooxygenase COX-1 with TNF- α and IL-6 inhibitors. *Saudi J. Biol. Sci.* **2020**, *27*, 1208–1216. [[CrossRef](#)]
18. Islam, M.S.; Al-Majid, A.M.; Azam, M.; Verma, V.P.; Barakat, A.; Haukka, M.; Elgazar, A.A.; Mira, A.; Badria, F.A. Construction of spirooxindole analogues engrafted with indole and pyrazole scaffolds as acetylcholinesterase inhibitors. *ACS Omega* **2021**, *6*, 31539–31556. [[CrossRef](#)]
19. Zhou, L.-M.; Qu, R.-Y.; Yang, G.-F. An overview of spirooxindole as a promising scaffold for novel drug discovery. *Expert Opin. Drug Discov.* **2020**, *15*, 603–625. [[CrossRef](#)]
20. Alshahrani, S.; Al-Majid, A.M.; Ali, M.; Alamar, A.S.; Abu-Serie, M.M.; Dömling, A.; Shafiq, M.; Ul-Haq, Z.; Barakat, A. Rational Design, Synthesis, Separation, and Characterization of New Spirooxindoles Combined with Benzimidazole Scaffold as an MDM2 Inhibitor. *Separations* **2023**, *10*, 225. [[CrossRef](#)]
21. Domingo, L.R. Molecular Electron Density Theory: A Modern View of Reactivity in Organic Chemistry. *Molecules* **2016**, *21*, 1319. [[CrossRef](#)]
22. Parr, R.G.; Yang, W. *Density Functional Theory of Atoms and Molecules*; Oxford University Press: New York, NY, USA, 1989.
23. Ríos-Gutiérrez, M.; Domingo, L.R. Unravelling the Mysteries of the [3+2] Cycloaddition Reactions. *Eur. J. Org. Chem.* **2019**, *2019*, 267–282. [[CrossRef](#)]
24. Domingo, L.R.; Ríos-Gutiérrez, M.; Pérez, P. Applications of the conceptual density functional indices to organic chemistry reactivity. *Molecules* **2016**, *21*, 748. [[CrossRef](#)] [[PubMed](#)]
25. Domingo, L.R.; Ríos-Gutiérrez, M. Application of Reactivity Indices in the Study of Polar Diels–Alder Reactions. In *Conceptual Density Functional Theory: Towards a New Chemical Reactivity Theory*; Liu, S., Ed.; WILEY-VCH GmbH: Weinheim, Germany, 2022; Volume 2, pp. 481–502.
26. Parr, R.G.; Pearson, R.G. Absolute hardness: Companion parameter to absolute electronegativity. *J. Am. Chem. Soc.* **1983**, *105*, 7512–7516. [[CrossRef](#)]
27. Domingo, L.R. A new C–C bond formation model based on the quantum chemical topology of electron density. *RSC Adv.* **2014**, *4*, 32415–32428. [[CrossRef](#)]
28. Domingo, L.R.; Ríos-Gutiérrez, M. A Useful Classification of Organic Reactions Based on the Flux of the Electron Density. *Sci. Rad.* **2023**, *2*, 1. [[CrossRef](#)]
29. Parr, R.G.; Szentpaly, L.V.; Liu, S. Electrophilicity index. *J. Am. Chem. Soc.* **1999**, *121*, 1922–1924. [[CrossRef](#)]
30. Ríos-Gutiérrez, M.; Saz Sousa, A.; Domingo, L.R. Electrophilicity and nucleophilicity scales at different DFF computational levels. *J. Phys. Org. Chem.* **2023**, *36*, e4503. [[CrossRef](#)]
31. Domingo, L.R.; Chamorro, E.; Pérez, P. Understanding the reactivity of captodative ethylenes in polar cycloaddition reactions. A theoretical study. *J. Org. Chem.* **2008**, *73*, 4615–4624. [[CrossRef](#)]
32. Domingo, L.R.; Pérez, P.; Sáez, J.A. Understanding the local reactivity in polar organic reactions through electrophilic and nucleophilic Parr functions. *RSC Adv.* **2013**, *3*, 1486–1494. [[CrossRef](#)]
33. Islam, M.S.; Al-Majid, A.M.; Haukka, M.; Parveen, Z.; Ravaiz, N.; Wadood, A.; Rehman, A.U.; Ríos-Gutiérrez, M.; Domingo, L.R.; Barakat, A. A novel alpha-amylase inhibitor-based spirooxindole-pyrrolidine-clubbed thiochromene-pyrzaole pharmacophores: Unveiling the [3+2] cycloaddition reaction by molecular electron density theory. *Chem. Biol. Drug. Des.* **2023**, *102*, 972–995. [[CrossRef](#)]
34. Evans, M.G.; Polanyi, M. Some applications of the transition state method to the calculation of reaction velocities, especially in solution. *Trans. Faraday Soc.* **1935**, *31*, 875–894. [[CrossRef](#)]
35. Fukui, K. Formulation of the reaction coordinate. *J. Phys. Chem.* **1970**, *74*, 4161–4163. [[CrossRef](#)]
36. Domingo, L.R.; Sáez, J.A.; Zaragoza, R.J.; Arnó, M. Understanding the Participation of Quadracyclane as Nucleophile in Polar Cycloadditions toward Electrophilic Molecules. *J. Org. Chem.* **2008**, *73*, 8791–8799. [[CrossRef](#)] [[PubMed](#)]

Disclaimer/Publisher's Note: The statements, opinions and data contained in all publications are solely those of the individual author(s) and contributor(s) and not of MDPI and/or the editor(s). MDPI and/or the editor(s) disclaim responsibility for any injury to people or property resulting from any ideas, methods, instructions or products referred to in the content.